Theor Chem Acc (2012) 131:1194
DOI 10.1007/s00214-012-1194-y

REGULAR ARTICLE

Multiconfigurational study on the synchronous mechanisms of the ClO self-reaction leading to Cl or Cl_2

Qingyong Meng · Hua Dong · Ming-Bao Huang

Received: 7 November 2011 / Accepted: 14 February 2012 / Published online: 2 March 2012

Abstract For studying the adiabatic and nonadiabatic mechanisms of the ClO ($X\ ^2\Pi$) + ClO ($X\ ^2\Pi$) → ClOOCl → 2Cl (^2P_u) + O_2 ($X\ ^3\Sigma_g^-$) reaction (1) and the ClO ($X\ ^2\Pi$) + ClO ($X\ ^2\Pi$) → ClOOCl → Cl_2 ($X\ ^1\Sigma_g^+$) + O_2 ($X\ ^3\Sigma_g^-$) reaction (2), we calculated, by partial geometry optimizations under the C_2 constraint, the O–O and O–Cl dissociation potential energy curves (PECs) from the five low-lying states of ClOOCl at the CASPT2 level. The CASSCF minimum-energy crossing point (MECP) between the potential energy surfaces of the 1 ^{1}A ground state [correlating with the product of reaction (1)] and the 1 ^{3}B state [correlating with the product of reaction (2)] states was also determined. Based on the CAS calculation results (PECs, energies, and spin–orbit coupling at the MECP), we predict that reaction (1) occurs along pathway 1: ClO ($X\ ^2\Pi$) + ClO ($X\ ^2\Pi$) → ClOOCl ($1\ ^1$A) → 2Cl (^2P_u) + O_2 ($X\ ^3\Sigma_g^-$) and that reaction (2) occurs along pathway 2: ClO ($X\ ^2\Pi$) + ClO ($X\ ^2\Pi$) → ClOOCl ($1\ ^1$A) → $1\ ^1$A/$1\ ^3$B MECP (142.4 cm^{-1}) → ClOOCl ($1\ ^3$B) → Cl_2 ($X\ ^1\Sigma_g^+$) + O_2 ($X\ ^3\Sigma_g^-$). The needed energies (relative to the reactant) for pathways 1 and 2 are predicted to be 5.3 and 11.1 kcal/mol, respectively, which indicates that reaction (1) is more favorable than reaction (2). The present work supports the traditional photochemical model for ozone degradation: ClOOCl ($1\ ^1$A), formed by two ClO ($X\ ^2\Pi$), can directly produce O_2 plus two Cl atoms.

Keywords ClOOCl · Adiabatic and nonadiabatic mechanisms · CASPT2 · MECP · Ozone degradation

Q. Meng (✉) · H. Dong · M.-B. Huang
College of Chemistry and Chemical Engineering,
Graduate University of Chinese Academy of Sciences,
P.O. Box 4588, Beijing 100049, People's Republic of China
e-mail: meng.tsiyong@gmail.com

1 Introduction

The traditional chlorine catalytic cycle for ozone hole formation [1–8] consists of the following reactions: (1) Cl + O_3 → ClO + O_2 (a simple reaction, but the key reaction for ozone degradation), (2) two ClO radicals in the ground state combine to form ClOOCl, and (3) ClOOCl dissociates into two Cl (^2P_u) atoms and O_2 ($X\ ^3\Sigma_g^-$) synchronously or stepwisely (via other isomers of ClOOCl or some intermediates). In the present work, we focus on the synchronous reaction from ClO, ClO ($X\ ^2\Pi$) + ClO ($X\ ^2\Pi$) → ClOOCl → 2Cl (^2P_u) + O_2 ($X\ ^3\Sigma_g^-$), which is denoted as reaction (1) in the present work. Because of the lower energy of Cl_2 ($X\ ^1\Sigma_g^+$) + O_2 ($X\ ^3\Sigma_g^-$), we also consider the reaction ClO ($X\ ^2\Pi$) + ClO ($X\ ^2\Pi$) → ClOOCl → Cl_2 ($X\ ^1\Sigma_g^+$) + O_2 ($X\ ^3\Sigma_g^-$), which is denoted as reaction (2) in the present work.

Reactions (1) and (2) have different final products, and the ClOOCl species in the above two equations may be in different electronic states. Each of reactions (1) and (2) can be considered to consist of O–O and O–Cl dissociation reactions from ClOOCl in a specific electronic state to the reactant (ClO + ClO) and final product (2Cl + O_2 or Cl_2 + O_2), respectively.

Extensive experimental [9–20] and theoretical [21–32] studies on the UV/Vis absorption spectrum of ClOOCl have been reported in the literature. Many recent experimental studies [6, 7, 14–20] have restored confidence in the traditional photochemical model for ozone degradation. To the best of our knowledge, no theoretical studies on reactions (1) and (2) have been reported in the literature. In 2003, Zhu and Lin [33] reported their theoretical mechanisms of ClO + ClO → Cl_2O_2 → Cl + ClOO and Cl_2 + O_2 via an isomer of ClOOCl using the B3LYP and Gaussian-2 methods. Multiconfigurational methods are

needed in theoretical study of reactions (1) and (2), since the open-shell systems appear in the reactant (ClO + ClO) and products, and the electronic excited states of ClOOCl may be involved. The main purpose of the present theoretical work is to study the adiabatic and nonadiabatic mechanisms of reactions (1) and (2), using the multiconfiguration second-order perturbation theory (CASPT2) [34, 35] and the complete active space self-consistent-field (CASSCF) [36] methods.

In the present study, we first calculated vertical excitation energies (T_v) at the CASPT2 level for many electronic states of ClOOCl using CASPT2 optimized geometry of the 1 ^{1}A ground state (see Sect. 3.1). We chose the 1 ^{1}A, 1 ^{1}B, 1 ^{3}A, 1 ^{3}B, and 2 ^{1}A states for further calculations, as these states are considered to be low-lying states [30–32] By performing CASPT2 partial geometry optimization calculations, we calculated the O–O and O–Cl dissociation potential energy curves (PECs) from ClOOCl in the five states to the ClO + ClO, 2Cl + O_2, or Cl_2 + O_2 group (see Sect. 3.2). The starting points of these O–O and O–Cl dissociation PECs are at the CASPT2 geometry of the 1 ^{1}A state, since the 1 ^{1}B, 1 ^{3}A, 1 ^{3}B, and 2 ^{1}A states are not bound states (indicated by our CASPT2 geometry optimization calculations and by the previous sa-CASSCF calculations of Kaledin and Morokuma [25]). This implies that the 1 ^{1}B, 1 ^{3}A, 1 ^{3}B, and 2 ^{1}A "adiabatic" paths for reactions (1) and (2) are assumed to pass through the geometry of the 1 ^{1}A state. For studying nonadiabatic paths, we located minimum-energy crossing points (MECPs) in the potential energy surfaces (PESs) between different states at the CASSCF level and calculated the CASPT2 energies and CASSCF spin–orbit coupling values at the MECPs. On the basis of our results, we predict adiabatic and nonadiabatic mechanisms of reactions (1) and (2). We will discuss the predicted mechanisms and also the above-mentioned assumption.

2 Technical details of calculation

Geometry and atom labeling used for ClOOCl are shown in Fig. 1. We assume that the reaction system (ClOOCl) remains in the C_2 symmetry.

The CAS calculations were carried out using the MOLCAS v7.4 package [37, 38]. A large contracted atomic natural orbital (ANO-L) basis set [39–42], Cl [5s4p3d2f]/O [4s3p2d1f], was used. With a CASSCF wave function constituting the reference function, the CASPT2 calculations were performed to compute the first-order wave function and the second-order energy in full CI space.

In the CASPT2 calculations for the electronic states of ClOOCl, 26 electrons were active and the active space included 16 orbitals (the full valence active space) [denoted as CASPT2 (26, 16)]. In the CAS calculations for the PECs and MECPs, 18 electrons were active and the active space included 12 orbitals (including all the *p*-orbitals of the four atoms) [denoted as CASSCF (18, 12) and CASPT2 (18, 12)]. Geometry optimization calculations for the 1 ^{1}A ground state were also performed at the CAS (18, 12) levels. In all the CASPT2 calculations, the weight values of the CASSCF reference functions in the first-order wavefunctions were larger than 0.80.

The O–O and O–Cl dissociation PECs of the five ClOOCl states were obtained based on the CASPT2 (18, 12) partial geometry optimization calculations performed at sets of fixed O–O and O–Cl bond distance values, respectively, ranging from the respective bond values in the CASPT2 (18, 12) 1 ^{1}A geometry (see Sect. 3.1) to 5.0 Å. The ClOOCl systems in the different states at the *R* (O–O) and *R* (O–Cl) values of 5.0 Å are called asymptote reactant (ClO + ClO) and asymptote products (2Cl + O_2 and Cl_2 + O_2), respectively. The CASSCF MECP calculations for selected state/state pairs were carried out in the C_2 symmetry. The state/state pairs were selected mainly based on the PEC crossings in the PEC figure.

All of the energy values reported in the present article do not include the zero-point energy (ZPE) corrections.

3 Results and discussion

3.1 Electronic states of ClOOCl

Given in Table 1 are the CASPT2 (26, 16) and (18, 12) optimized geometries (in the C_2 symmetry) for the ground state (1 ^{1}A) of ClOOCl, together with the previously reported theoretical [30] and experimental [10, 11] geometric data. The predicted C_2 equilibrium geometry was confirmed by the CASSCF (18, 12) frequency calculations using the CASSCF (18, 12) optimized geometry. The CASPT2 (26, 16) geometries are very close to the respective CASPT2 (18, 12) geometries. As shown in Table 1, deviations of the CASPT2 geometric parameter values from the respective experimental values are within 0.04 Å for bond lengths and 0.9° for bond angle and dihedral angle. The previous CCSD (T) calculations [30] predicted a more accurate 1 ^{1}A geometry than our CASPT2 calculations and the previous MRCI calculations [30]. The discrepancies among these theoretical geometries should

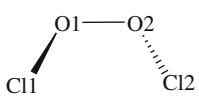

Fig. 1 Atom labelings for ClOOCl in the C_2 and C_s symmetry, respectively, used in the present work

Table 1 CASPT2 (26, 16) and CASPT2 (18, 12) optimized geometries for the 1 ^{1}A ground state of the ClOOCl molecule, together with the previously reported theoretical and experimental geometries (bond lengths are given in Å, the angle and dihedral values in degrees; for notations see Fig. 2)

Calculation methods	1 ^{1}A geometry			
	R (O–O)	R (O–Cl)	∠ClOO	∠ClOOCl
CASPT2 (26, 16)	1.383	1.732	109.2	81.1
CASPT2 (18, 12)	1.386	1.730	109.2	82.3
MRCI (26, 16)[a]	1.396	1.775	109.4	84.8
CASSCF (18, 12)[b]	1.354	1.826	110.7	86.4
CCSD (T)[a]	1.406	1.715	109.4	82.6
Experimental geometry[c]	1.426	1.704	110.1	81.9

[a] Ref. [30]

[b] Ref. [25]

[c] Refs. [10, 11]

be caused by the different electronic correlation methods, different active spaces, and/or different basis sets.

The T_v values for eight low-lying (singlet and triplet) states of ClOOCl were calculated at the CASPT2 levels, and the 1 ^{1}A (ground state), 1 ^{1}B, 1 ^{3}A, 1 ^{3}B, and 2 ^{1}A states are predicted to be the five lowest-lying states. Given in Table 2 are the CASPT2 (26, 16) T_v values of the five states [based on the CASPT2 (26, 16) energy calculations using the optimized 1 ^{1}A geometry at the CASPT2 (26, 16) level] and the CASPT2 (18, 12) T_v values of the five states [based on the CASPT2 (18, 12) energy calculations using the optimized 1 ^{1}A geometry at the CASPT2 (18, 12) level]. The CASPT2 (26, 16) T_v values of the 1 ^{1}A, 1 ^{1}B, 1 ^{3}A, 1 ^{3}B, and 2 ^{1}A states are 0.0, 3.47, 2.75, 2.73, and 3.50 eV, respectively. The experimental T_v values are not available.

The CASPT2 (18,12) T_v values (0.0, 3.49, 2.78, 2.76, and 3.53 eV for 1 ^{1}A, 1 ^{1}B, 1 ^{3}A, 1 ^{3}B, and 2 ^{1}A, respectively) are very close to the respective CASPT2 (26,16) T_v values. The T_v values of the five states based on the CASPT2 (26, 16) energy calculations using the 1 ^{1}A experimental geometry (see Table 1) are also given in Table 2, and they are only slightly larger than the CASPT2 (26, 16) T_v values (though the bond length values in the CASPT2 (26, 16) 1 ^{1}A optimized geometry are not very close to the experimental values). In Table 2, we also list some previously reported theoretical T_v values [30–32], which are larger (or significantly larger) than the CASPT2 T_v values. As already mentioned, the 1 ^{1}B, 1 ^{3}A, 1 ^{3}B, and 2 ^{1}A states are not bound states (indicated by our CASPT2 geometry optimization calculations and CASSCF//CASSCF vibrational frequency analyses and by the previous sa-CASSCF calculations [25]).

Table 2 CASPT2 (26, 16) and CASPT2 (18, 12) vertical excitation energies (T_v, in eV) for the five low-lying (singlet and triplet) states of the ClOOCl molecule [based on the CASPT2 (26, 16) and CASPT2 (18, 12) energy calculations at the CASPT2 (26, 16) and CASPT2 (18, 12) optimized geometries of the 1 ^{1}A ground state, respectively], together with previously reported T_v values calculated using multi-configurational methods

Calculation level	T_v				
	1 ^{1}A	1 ^{3}B	1 ^{3}A	1 ^{1}B	2 ^{1}A
CASPT2 (26, 16)	0.0	2.73	2.75	3.47	3.50
CASPT2 (18, 12)	0.0	2.76	2.78	3.49	3.53
CASPT2 (26, 16)[a]	0.0	2.79	2.82	3.55	3.58
sa-CASPT2 (20, 13)[b]	0.0			3.75	3.78
MRCI (20, 13)[b]	0.0			4.00	4.01
MRCI (26, 16)[c]	0.0	3.12	3.12	4.04	4.04
CASSCF (26, 16)[d]	0.0	3.15	3.21	4.32	4.37
EOM-CCSD[e]	0.0			3.80	3.83

[a] The present work. Calculated at the experimental geometry (see Table 1) of the 1 ^{1}A ground state

[b] Ref. [31]. Calculated at the MP2 geometry of the ground state [R (O–O) = 1.419 Å, R (O–Cl) = 1.744 Å, ∠ClOO = 109.0°, and ∠ClOOCl = 85.0°]

[c] Ref. [32]. Calculated at the CCSD (T) geometry (see Table 1) of the 1 ^{1}A ground state

[d] Ref. [30]. Calculated at the CCSD (T) geometry (see Table 1) of the 1 ^{1}A ground state

[e] Ref. [25]. Calculated at the CASSCF geometry (see Table 1) of the 1 ^{1}A ground state

3.2 O–O and O–Cl dissociation potential energy curves from ClOOCl

Given in Fig. 2 (the PEC figure) are the O–O and O–Cl dissociation PECs for the 1 ^{1}A, 1 ^{1}B, 1 ^{3}A, 1 ^{3}B, and 2 ^{1}A states of ClOOCl at the CASPT2 (18, 12) level, the starting points of these O–O and O–Cl dissociation PECs are the the CASPT2 (18, 12) 1 ^{1}A geometry (mentioned in Introduction). In Fig. 2, we also give the CASPT2 (18, 12) energy values (relative to 1 ^{1}A) of asymptote reactant (ClO + ClO) and asymptote products (2Cl + O_2 and Cl_2 + O_2) in the five ClOOCl states. In the following text, "the CASPT2 (18, 12) energy values (relative to 1 ^{1}A)" will be abbreviated to "the CASPT2 energy values." Similar singlet PECs were reported in the previous CASSCF [25], CAS-CI [27], and MRCI [32] studies (however, the triplet PECs were not calculated in those studies). Those singlet PECs were obtained based on single-point energy calculations and did not represent minimum-energy paths.

Based on the CASPT2 geometry optimization calculations for ClO ($X\ ^2\Pi$), Cl_2 ($X\ ^1\Sigma_g^+$), and O_2 ($X\ ^3\Sigma_g^-$) (the optimized bond length values being 1.571, 1.999, and 1.206 Å, respectively) and the CASPT2 energy calculations

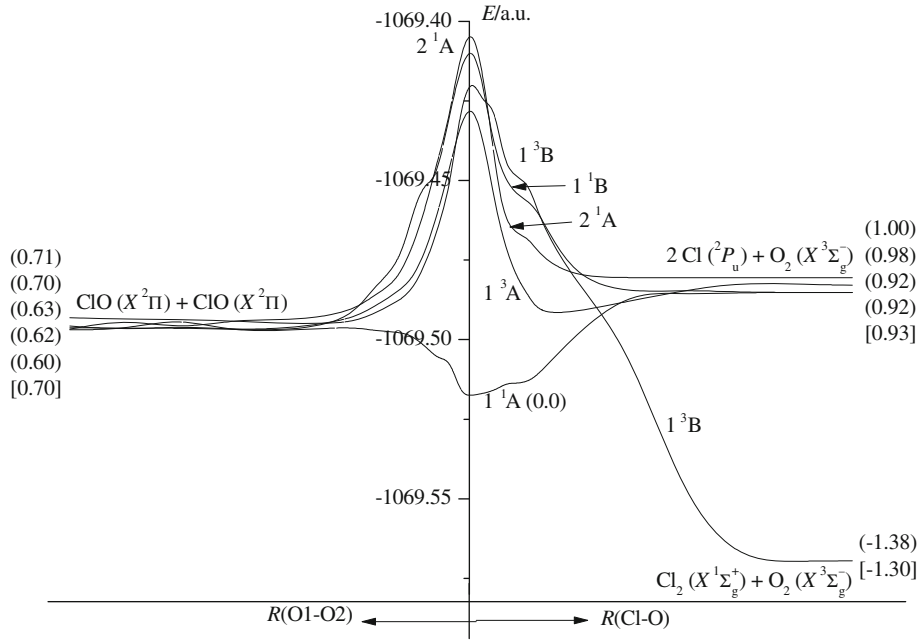

Fig. 2 CASPT2 (18, 12) PECs of the 1 ^{1}A, 1 ^{1}B, 1 ^{3}A, 1 ^{3}B, and 2 ^{1}A states of ClOOCl for the O–O dissociation [to the reactant of reactions (1) and (2)] and for the O–Cl dissociation [to the products of reactions (1) and (2)]. Values in parentheses are the CASPT2 (18, 12) energies (in eV, relative to 1 ^{1}A) of the asymptote reactants and products in the five ClOOCl states, and values in *square brackets* are the CASPT2 (18, 12) sum energies (in eV, relative to 1 ^{1}A) for the reactant and products of reactions (1) and (2). We incorporate the O–O and Cl–O dissociation PECs of the five states in this figure. The starting values along the left-hand and right-hand horizontal axes are the R (O–O) (1.386 Å) and R (Cl–O) (1.730 Å) values in the CASPT2 (18, 12) optimized geometry of ClOOCl (1 ^{1}A), respectively

for Cl (^2P_u), we evaluated the CASPT2 sum energy values (relative to 1 ^{1}A) for the ClO (X $^2\Pi$) + ClO (X $^2\Pi$) (reactant), 2Cl (^2P_u) + O_2 (X $^3\Sigma_g^-$) (product), and Cl_2 (X $^1\Sigma_g^+$) + O_2 (X $^3\Sigma_g^-$) (product). These evaluated values are 0.70, 0.93, and −1.30 eV, respectively, and are given in Table 3 and in Fig. 2. By "sum energy," we mean the sum [relative to ClOOCl (1 ^{1}A)] of the calculated energies of the species in the reactant group or in the product groups. For example, the sum energy of the reactant group = 2 × the calculated total energy value of ClO (X $^2\Pi$) at its optimized geometry minus the calculated total energy value of ClOOCl (1 ^{1}A) at its optimized geometry. The previously reported experimental [2, 7, 20, 43] and theoretical [25, 27] sum energy values (relative to 1 ^{1}A) are listed in Table 3. The CASPT2 sum energy value of 0.70 eV for ClO (X $^2\Pi$) + ClO (X $^2\Pi$) is in good agreement with the experimental sum energy values of 0.74 eV [2], 0.71 eV [20], and 0.77 eV [7]. The CASPT2 sum energy value of 0.93 eV for 2Cl (^2P_u) + O_2 (X $^3\Sigma_g^-$) is in agreement with the experimental sum energy values of 1.17 eV [2] and 1.09 eV [20]. The CASPT2 sum energy value of −1.30 eV for Cl_2 (X $^1\Sigma_g^-$) + O_2 (X $^3\Sigma_g^-$) is in good agreement with the experimental sum energy values of −1.31 eV [43]. The previously reported CAS-CI sum energy value (0.76 eV) [27]. for ClO (X $^2\Pi$) + ClO (X $^2\Pi$) is also in good agreement with experiment [2, 7, 20] but the other three sum energy values predicted by the previous theoretical studies [25, 27] are not in good agreement with experimental results [2, 7, 20] (one of the three values has a wrong sign).

We first analyze the O–O dissociation PECs in the left part of Fig. 2. The CASPT2 energy values of the 1 ^{1}A, 1 ^{1}B, 1 ^{3}A, 1 ^{3}B, and 2 ^{1}A asymptote reactants (0.60, 0.62, 0.71, 0.63, and 0.70 eV, respectively) are close to the CASPT2 sum energy value of 0.70 eV for the ClO (X $^2\Pi$) + ClO (X $^2\Pi$) reactant group. The Cl–O bond length values in all the five asymptote reactants are close to the bond length value (1.571 Å) in the CASPT2 optimized geometry of ClO (X $^2\Pi$). These facts indicate that the 1 ^{1}A, 1 ^{1}B, 1 ^{3}A, 1 ^{3}B, and 2 ^{1}A states of ClOOCl correlate with ClO (X $^2\Pi$) + ClO (X $^2\Pi$) [the reactant of reactions (1) and (2)]. Along the 1 ^{1}A PEC, the energy monotonocally increases with the O–O distance. The 1 ^{1}B, 1 ^{3}A, 1 ^{3}B, and 2 ^{1}A PECs are essentially repulsive.

We then analyze the O–Cl dissociation PECs in the right part of Fig. 2. The CASPT2 energy value (−1.38 eV) of the 1 ^{3}B asymptote product is very close to the CASPT2 sum energy value of −1.30 eV for the Cl_2 (X $^1\Sigma_g^+$) + O_2 (X $^3\Sigma_g^-$) product group. The Cl–Cl and O–O bond length values (1.983 and 1.212 Å, respectively) in the 1 ^{3}B asymptote product are close to the bond length values (1.999 and 1.206 Å) in the CASPT2 optimized geometries of Cl_2 (X $^1\Sigma_g^+$) and O_2 (X $^3\Sigma_g^-$), respectively. These facts indicate that the 1 ^{3}B state of ClOOCl correlates with Cl_2 (X $^1\Sigma_g^+$) + O_2 (X $^3\Sigma_g^-$) [the product of reaction (2)]. The

Table 3 CASPT2 (18, 12) sum energy values [ΔE, in eV, relative to ClOOCl ($1\,^1A$)] of the reactant and product groups for reactions (1) and (2), together with the previously reported theoretical and experimental sum energy values

Groups	ΔE				States of ClOOCl in C_2 symmetry[c]
	CASPT2	CASSCF[a]	CAS-CI[b]	Experiment	
Reactant group					
ClO ($X\,^2\Pi$) + ClO ($X\,^2\Pi$)	0.70	1.10	0.76	0.74[d], 0.71[e], 0.77[f]	Two ^{1,3}A, two ^{1,3}B ($1\,^{1,3}$A, $1\,^{1,3}$B, $2\,^1$A)
Product groups					
Cl_2 ($X\,^1\Sigma_g^+$) + O_2 ($X\,^3\Sigma_g^-$)	−1.30			−1.31[g]	One ^{3}B ($1\,^3$B)
2Cl (^2P_u) + O_2 ($X\,^3\Sigma_g^-$)	0.93	−0.10	0.41	1.17[d], 1.09[e]	Four ^{1,3,5}A, five ^{1,3,5}B ($1\,^1$A, $2\,^1$A, $1\,^1$B, $1\,^3$A)

[a] Ref. [25]

[b] Ref. [27]

[c] In parentheses are the ClOOCl states calculated in the present work

[d] Ref. [2]

[e] Ref. [20]

[f] Ref. [7]

[g] Ref. [43]

CASPT2 energy values of the $1\,^1$A, $1\,^1$B, $1\,^3$A, and $2\,^1$A asymptote products (0.92, 0.92, 0.98, and 1.00 eV, respectively) are close to the CASPT2 sum energy value of 0.93 eV for the 2Cl (^2P_u) + O_2 ($X\,^3\Sigma_g^-$) product group. The O–O bond length values (1.229, 1.218, 1.219, and 1.209 Å) in the four asymptote products are close to the bond length value of 1.206 Å in the CASPT2 optimized geometry of O_2 ($X\,^3\Sigma_g^-$), and the distance values between the two Cl atoms (8.666, 7.052, 6.954, and 5.167 Å) in the four asymptote products are very large. These facts indicate that the $1\,^1$A, $1\,^1$B, $1\,^3$A, and $2\,^1$A states of ClOOCl correlate with 2Cl (^2P_u) + O_2 ($X\,^3\Sigma_g^-$) [the product of reaction (1)]. Along the $1\,^1$A PEC, the energy monotonically increases with the O–Cl distance. Along the $1\,^3$A PEC, there is a shallow minimum. The $1\,^1$B, $1\,^3$B, and $2\,^1$A PECs are essentially repulsive.

There seem to be transition states in the $1\,^1$B, $1\,^3$A, $1\,^3$B, and $2\,^1$A PESs in regions around the $1\,^1$A geometry (see Fig. 2), and they could be used as the starting points of the O–O and O–Cl dissociation PECs of the four excited states. However, we failed to locate the expected transition states. Since the starting points of the O–O and O–Cl dissociation PECs in Fig. 2 are just the $1\,^1$A geometry, the continuous $1\,^1$B, $1\,^3$A, $1\,^3$B, and $2\,^1$A paths form the reactant to products in Fig. 2 do not represent adiabatic reaction paths in the IRC sense. However, we will see in Sect. 3.5 that these problems are not important and can be ignored.

3.3 The $1\,^1$A/$1\,^3$B MECPs

As shown in the right part of Fig. 2, the $1\,^3$B PEC crosses the $1\,^1$A, $1\,^1$B, $1\,^3$A, and $2\,^1$A PECs. We only considered the $1\,^1$A/$1\,^3$B MECPs since the $1\,^1$A state is the ground state and the $1\,^1$A/$1\,^3$B PEC crossing point is low in energy in Fig. 2. The $1\,^3$A/$1\,^3$B PEC crossing point is also low in energy, but the spin–orbit coupling value at the CASSCF $1\,^3$A/$1\,^3$B MECP was calculated to be zero.

At the CASSCF (18, 12) level, we located two MECPs between the $1\,^1$A and $1\,^3$B PESs. One MECP has a ClOOCl dihedral angle value of 176.2° in its geometry and is denoted as *anti*-MECP. The other MECP has a ClOOCl dihedral angle value of 0.0° in its geometry and is denoted as *syn*-MECP. The two MECPs are considered as two minima in the seam (a 5-D hypersurface) between the $1\,^1$A and $1\,^3$B PESs. The CASSCF (18, 12) energy differences between the $1\,^1$A and $1\,^3$B states at the *syn*-MECP and *anti*-MECP are 2.4×10^{-7} and 2.9×10^{-7} a.u., respectively.

Given in Table 4 are the CASSCF (18, 12) geometries for the two MECPs, the CASSCF (18, 12) spin–orbit couplings, and CASPT2 (18, 12) energies of the $1\,^1$A/$1\,^3$B states ($\Delta E/\Delta E$, relative to $1\,^1$A) calculated using the CASSCF (18, 12) MECPs geometries. The large R (O–Cl) values in the two MECP geometries indicate that the optimized MECPs lie along the way in the O–Cl dissociations. According to the geometries of the two MECPs, the *syn*-MECP may play a role in $1\,^3$B ← $1\,^1$A intersystem crossing leading to the product (Cl_2 + O_2) of reaction (2), while the *anti*-MECP may play a role in $1\,^1$A ← $1\,^3$B intersystem crossing (involved in a process: $1\,^3$B → *anti*-MECP → $1\,^1$A → 2Cl + O_2). For studying nonadiabatic mechanism of reaction (2), we will only consider the $1\,^1$A/$1\,^3$B *syn*-MECP. The CASSCF (18, 12) spin–orbit coupling values at the two MECPs are very large. The CASPT2 (18, 12) energy differences between the two states at the two CASSCF MECPs are both 0.29 eV, and in the following discussion, we will use the CASPT2 (18, 12)//CASSCF (18, 12) average energy values. The CASPT2 (18, 12) average energy values (relative to

Table 4 Located MECPs (MECPs) between the 1 ^{1}A and 1 ^{3}B PESs at the CASSCF (18, 12) level: *syn*-MECP and *anti*-MECP

1 ^{1}A/1 ^{3}B MECP	Geometry					Spin–orbit coupling	CASPT2 $\Delta E/\Delta E$[b]
	R (O–Cl)	*R* (O1–O2)	*R* (Cl1–Cl2)	∠ClOO	∠ClOOCl		
Syn-MECP	2.384	1.159	3.066	113.6	0.0	142.4	1.04/1.33 (1.18)
Anti-MECP	2.242	1.152	5.198	122.7	176.2	153.6	1.21/1.49 (1.35)

The given results are the CASSCF (18, 12) MECP geometries[a] (bond lengths are given in Å, bond angles and dihedral in degrees) and the CASSCF (18, 12) spin–orbit couplings (in cm^{-1}) and CASPT2 (18, 12) energies of the 1 ^{1}A/1 ^{3}B states ($\Delta E/\Delta E$ in eV, relative to 1 ^{1}A) calculated at the CASSCF (18, 12) MECPs. The *syn*-MECP is considered in the 1 ^{3}B ← 1 ^{1}A intersystem crossing of reaction (2), while the *anti*-MECP should be considered in the 1 ^{1}A ← 1 ^{3}B intersystem crossing

[a] The CASSCF (18, 12) energy differences between the 1 ^{1}A and 1 ^{3}B states at the two MECPs are small than 3.0×10^{-7} a.u.

[b] Values in parentheses are the averages

1 ^{1}A) at the *syn*-MECP and *anti*-MECP are 1.18 and 1.35 eV, respectively (the value at the *syn*-MECP being smaller than that at the *anti*-MECP).

3.4 The predicted mechanisms for reactions (1) and (2)

On the basis of our results (the CASPT2 PECs and the CASPT2 and CASSCF results at the MECPs), we are able to predict the reaction mechanisms. Reaction (1) is predicted to have the following adiabatic mechanism (pathway 1):

$$\begin{aligned}&\mathrm{ClO}\,(X^2\Pi) + \mathrm{ClO}\,(X^2\Pi)\,(0.70\,\mathrm{eV})\\ &\quad\rightarrow \mathrm{ClOOCl}\,(1^1\mathrm{A})\,(0.0\,\mathrm{eV})\\ &\quad\rightarrow 2\mathrm{Cl}\left(^2P_\mathrm{u}\right) + \mathrm{O}_2\left(X^3\Sigma_g^-\right)(0.93\,\mathrm{eV}).\end{aligned}$$

Reaction (2) is predicted to have the following nonadiabatic mechanism (pathway 2):

$$\begin{aligned}&\mathrm{ClO}\,(X^2\Pi) + \mathrm{ClO}(X^2\Pi)\,(0.70\,\mathrm{eV})\\ &\quad\rightarrow \mathrm{ClOOCl}(1^1\mathrm{A})(0.0\,\mathrm{eV})\\ &\quad\rightarrow 1^1\mathrm{A}/1^3\mathrm{B}\,syn\text{-MECP}\left(1.18\,\mathrm{eV}, 142.4\,\mathrm{cm}^{-1}\right)\\ &\quad\rightarrow \mathrm{ClOOCl}\left(1^3\mathrm{B}\right)\\ &\quad\rightarrow \mathrm{Cl}_2\left(X^1\Sigma_g^+\right) + \mathrm{O}_2\left(X^3\Sigma_g^-\right)(-1.30\,\mathrm{eV}).\end{aligned}$$

Values in parentheses are the CASPT2 (18, 12) energies of species along the pathways [relative to ClOOCl (1^{1}A)]. The value of 1.18 eV in the parenthesis after "*syn*-MECP" is the CASPT2 (18, 12)//CASSCF (18, 12) average energy value, and it is smaller than the CASPT2 (18, 12) T_v value (2.76 eV) of the 1 ^{3}B state. The spin–orbit coupling value of 142.4 cm^{-1} at the 1 ^{1}A/1 ^{3}B *syn*-MECP is large enough for 1 ^{3}B ← 1 ^{1}A intersystem crossing.

At the CASPT2 (18, 12) level, the needed energies from the reactant for pathway 1 (the maximum energy at the final product) and pathway 2 (the maximum energy at the *syn*-MECP) are predicted to be 0.23 eV (5.3 kcal/mol) and 0.48 eV (11.1 kcal/mol), respectively.

3.5 Conclusion and discussion

On the basis of our CASPT2 PEC and CASPT2//CASSCF MECP calculations, we predict that reaction (1) occurs along pathway 1: ClO ($X\,^2\Pi$) + ClO ($X\,^2\Pi$) → ClOOCl (1 ^{1}A) → 2Cl ($^2P_\mathrm{u}$) + O_2 ($X\,^3\Sigma_g^-$) and reaction (2) occurs along pathway 2: ClO ($X\,^2\Pi$) + ClO ($X\,^2\Pi$) → ClOOCl (1 ^{1}A) → 1 ^{1}A/1 ^{3}B *syn*-MECP (142.4 cm^{-1}) → ClOOCl (1 ^{3}B) → Cl_2 ($X\,^1\Sigma_g^+$) + O_2 ($X\,^3\Sigma_g^-$). The maximum energies along pathways 1 and 2 are at the product and the MECP, respectively. The maximum energy along pathway 1 is the energy at the product group 2Cl + O_2 (5.3 kcal/mol), and the maximum energy along pathway 2 is the energy at the 1 ^{1}A/1 ^{3}B *syn*-MECP (11.1 kcal/mol).

Multiconfigurational methods (e.g., CASSCF, CASPT2, and MRCI) are certainly needed, since there are open-shell species in the reactant and also in the products, and electronic excited states (of ClOOCl) may be involved. The CASPT2 sum energy values [relative to ClOOCl (1^{1}A)] for the reactant and product groups of the two reactions are close to the respective experimental sum energy values (see Table 3), indicating that the CASPT2 calculations are accurate and size-consistent. For the prediction of the mechanisms (pathways 1 and 2), we only need the O–O and O–Cl dissociation PECs of the 1 ^{1}A ground state, the O–Cl dissociation PEC of the 1 ^{3}B state, and the results at the 1 ^{1}A/1 ^{3}B MECP. Therefore, the problems concerning transition states in the 1 ^{1}B, 1 ^{3}A, 1 ^{3}B, and 2 ^{1}A excited states (see the last paragraph of Sect. 3.2) are not important and can be ignored.

The calculations for the MECPs are important in the present study. An automatic search for MECPs at the CASPT2 level is not possible at the present stage, but we consider that the predicted mechanism for reaction (2) (pathway 2, via the 1 ^{1}A/1 ^{3}B PES crossing) is reliable. The CASPT2//CASPT2 energy value at the 1 ^{1}A/1 ^{3}B *syn*-MECP is not known, and we hope that it will be smaller than the CASPT2 T_v value of the 1 ^{3}B state and larger than the CASPT2 sum energy value for 2Cl ($^2P_\mathrm{u}$) + O_2 ($X\,^3\Sigma_g^-$).

Our CASPT2 calculations predict that the needed energies (from the reactant) for pathways 1 and 2 [for reactions (1) and (2), respectively] are 5.3 and 11.1 kcal/mol, respectively, which are small or not large. Reaction (1) is energetically more favorable than reaction (2) though the product of reaction (2) is lower in energy than the product of reaction (1). Many previous experimental groups [14–20] have considered that the reactions are photochemical reactions. The present theoretical work supports the traditional photochemical model for ozone degradation by the ClOOCl ($1\ ^1A$) molecule. The ClOOCl molecule is formed by the self-reaction of two ClO ($X\ ^2\Pi$) and then it can directly produce O_2 ($X\ ^3\Sigma_g^-$) plus two Cl atoms (other isomers of ClOOCl or intermediates are not needed in the process from ClOOCl ($1\ ^1A$) to 2Cl). One Cl atom can drive more than one chlorine catalytic cycle for the ozone hole formation in the pole ozonosphere.

Acknowledgments We appreciate the financial support for this work that was provided by National Natural Science Foundation of China through Contract No. 20773161. We thank the anonymous referees for their constructive suggestions to improve the work.

References

1. Molina LT, Molina MJ (1987) J Phys Chem 91:433–436
2. Cox RA, Hayman GD (1988) Nature 332:796–800
3. Sander SP, Friedl RR, Yung YL (1989) Science 245:1095–1098
4. World Meteorological Organization (WMO) (2006) Scientific assessment of ozone depletion. WMO, global ozone research and monitoring project, report no. 50: Geneva, Switzerland, 2007, http://ozone.unep.org/Assessment_Panels/SAP/Scientific_Assessment_2006. Accessed Feb 2007
5. von Hobe M, Salawitch RJ, Canty T, Keller-Rudek H, Moortgat GK, Grooss J-U, Muller R, Stroh F (2007) Atmos Chem Phys 7:3055–3069
6. Santee ML, Sander SP, Livesey NJ, Froidevaux L (2010) PNAS 107(15):6588–6593. doi:10.1073/pnas.0912659107
7. Ferracci V, Rowley DM (2010) Phys Chem Chem Phys 12:11596–11608
8. Sander SP, Ravishankara AR, Golden DM, Kolb CE, Kurylo MJ, Molina MJ, Moortgat GK, Finlayson-Pitts BJ, Wine PH, Huie RE, Orkin VL (2006) Chemical kinetics and photochemical data for use in atmospheric studies. Evaluation no. 15, JPL publication 06-2. Jet Propulsion Laboratory, Pasadena
9. Trolier M, Mauldin RL III, Ravishankara AR (1990) J Phys Chem 94:4896–4907
10. Birk M, Friedl RR, Cohen EA, Pickett HM, Sander SP (1989) J Chem Phys 91:6588–6597
11. Jacobs J, Kronberg M, Müller HSP, Willner H (1994) J Am Chem Soc 116:1106–1114
12. Moore TA, Okumura M, Seale JW, Minton TK (1999) J Phys Chem A 103:1691–1695
13. Pope FD, Hansen JC, Bayes KD, Friedl RR, Sander SP (2007) J Phys Chem A 111:4322–4332
14. von Hobe M, Stroh F, Beckers H, Benter T, Willner H (2009) Phys Chem Chem Phys 11:1571–1580
15. Wilmouth DM, Hanisco TF, Stimpfle RM, Anderson JG (2009) J Phys Chem A 113:14099–14108
16. Papanastasiou DK, Papadimitriou VC, Fashey DW, Burkholder JB (2009) J Phys Chem A 113:13711–13726
17. Chen H-Y, Lien C-Y, Lin W-Y, Lee YT, Lin JJ (2009) Science 324:781–784
18. Lien C-Y, Lin W-Y, Chen H-Y, Huang W-T, Jin B, Chen C, Lin JJ (2009) J Chem Phys 131:174301
19. Jin B, Chen I-C, Huang W-T, Lien C-Y, Guchhait N, Lin JJ (2010) J Phys Chem A 114:4791–4797
20. Huang W-T, Chen AF, Chen I-C, Tsai C-H, Lin JJ (2011) Phys Chem Chem Phys 13:8195–8203
21. McGrath MP, Clemitshaw KC, Rowland FS, Hehre WJ (1990) J Phys Chem 94:6126–6132
22. Rendell AP, Lee TJ (1991) J Chem Phys 94:6219–6228
23. Lee TJ, Rohlfing CM, Rice JE (1992) J Chem Phys 97:6593–6605
24. Stanton JF, Bartlett RJ (1993) J Chem Phys 98:9335–9339
25. Kaledin AL, Morokuma K (2000) J Chem Phys 113:5750–5762
26. Toniolo A, Persico M, Pitea D (2000) J Phys Chem A 104:7278–7283
27. Toniolo A, Granucci G, Inglese S, Persico M (2001) Phys Chem Chem Phys 3:4266–4279
28. Tomasello P, Ehara M, Nakatsuji H (2002) J Chem Phys 116:2425–2432
29. Tomasello P, Ehara M, Nakatsuji H (2003) J Chem Phys 118:5811–5820
30. Peterson KA, Francisco JS (2004) J Chem Phys 121:2611–2616
31. Ončák M, Šištík L, Slavíček P (2010) J Chem Phys 133:174303
32. Grein F (2011) Chem Phys 382:34–40
33. Zhu RS, Lin MC (2003) J Chem Phys 118:4094–4106
34. Andersson K, Roos BO (1995) Multiconfigurational second-order perturbation theory. In: Yarkony DR (ed) Modern electronic structure theory, part 1. World Scientific, Singapore, p 55
35. Andersson K, Roos BO (1993) Int J Quantum Chem 45:591–607
36. Roos BO (1987) The complete active space self-consistent field method and its applications in electronic structure calculations. In: Lawley KP (ed) Advances in chemical physics. Wiley, New York, pp 399–445
37. Karlström G, Lindh R, Malmqvist P-Å, Roos BO, Ryde U, Veryazov V, Widmark P-O, Cossi M, Schimmelpfennig B, Neogrady P, Seijo L (2003) Comput Mater Sci 28:222
38. Aquilante F, De Vico L, Ferré N, Ghigo G, Malmqvist P-Å, Neogrády P, Pedersen TB, Pitoňák M, Reiher M, Roos BO, Serrano-Andrés L, Urban M, Veryazov V, Lindh R (2010) J Comput Chem 31:224–247
39. Almlof J, Taylor PR (1987) J Chem Phys 86:4070–4077
40. Pierloot K, Dumez B, Widmark P-O, Roos BO (1995) Theoret Chem Acc 90:87–114
41. Widmark P-O, Malmqvist P-Å, Roos BO (1990) Theoret Chem Acc 77:291–306
42. Widmark P-O, Persson BJ, Roos BO (1991) Theoret Chem Acc 79:419–432
43. Li J, Hao Y, Yang J, Zhou C, Mo Y (2007) J Chem Phys 127:104307